Special Issue on Proceedings of International Conference on Newer Trends and Innovation in Nanotechnology, Materials Science, Science and Technology March 2021. International Journal of Aquatic Science, Vol 12, Issue

# MODELLING AND ANALYSIS OF SHIELDED METAL ARC WELDED JOINTS

**Raja Subramanian, V and Balthilak**

Nehru Institute of Technology,

Kaliyapuram, Coimbatore 6411 05, Tamilnadu, India

**Correspondent Email: rishirajaraja@gmail.com**

**Abstract-**Arc welding involves in a localized heat application in the substrate plates. The uneven heat distribution causes defects which influence the desired properties of welded joint. This project is studied about the welding distortion residual stress and the temperature distribution in the butt joint of thin plates welding. Double ellipsoid heat source is generated and finite element analysis were carried out using finite element code - ANSYS software. Experimental analysis was carried out by varying thickness of plates and the input parameters like voltage and current. The effect of distortion, residual stress for the varying parameter was observed. Thermocouples were placed in different nodes of the plates for observing the temperature distribution in the respective measuring nodes. LAB VIEW software was used to display the thermal curves by using the collected signals from the thermocouples.

**Keywords:** welding, stress, voltage, current, thermocouples

## 1. Introduction:

Shielded Metal Arc Welding also known as manual metal arc welding, stick welding, or electric arc welding, is the most widely used of the various arc welding processes. Welding is performed with the heat of an electric arc that is maintained between the end of a coated metal electrode and the work piece (See Figure 1.1) The heat produced by the arc melts the base metal, the electrode core rod, and the coating. As the molten metal droplets are transferred cross the arc and into the molten weld puddle, they are shielded from the atmosphere by the gases produced from the decomposition of the flux coating. The molten slag floats to the top of the weld puddle where it protects the weld metal from the atmosphere during solidification.

The most important function of a coating is to shield the weld metal from the oxygen and nitrogen of the air as it is being transferred across the arc, and while it is in the molten state. This shielding is necessary to ensure the weld metal will be sound, free of gas pockets, and have the right strength and ductility. At the high temperatures of the arc, nitrogen and oxygen combine readily with iron to a form iron nitrides and iron oxides that, if present in the weld metal above certain minimum amounts, will cause brittleness and porosity. Nitrogen is the primary concern since it is difficult to control its effect once it has entered the deposit. Oxygen can be counteracted by the use of suitable deoxidizers. In order to avoid contamination from the air, the stream of molten metal must be protected or shielded by gases that exclude the surrounding atmosphere from the arc and the molten weld metal. This is accomplished by using gas-forming materials in the coating that break down during the welding operation and produce the gaseous shield.

The actual welding technique utilized depends on the electrode, the composition of the work piece, and the position of the joint being welded. The choice of electrode and welding position also determine the welding speed. Flat welds require the least operator skill, and can be done with electrodes that melt quickly but solidify slowly. This permits higher welding speeds. Sloped, vertical or upside-down welding requires more operator skill, and often necessitates the use of an electrode that solidifies quickly to prevent the molten metal from flowing out of the weld pool.

## Proposed System:

Shielded metal arc welding is one of most widely used welding process, in which many research work have been attempted in metallurgical characterization and predicting results like temperature distribution, residual stress and distortion on structural steel. Simulation of welding process will reduce the time in production planning. The SYSWELD is one of the few dedicated software for the welding simulation. So the shielded metal arc

welding is simulated for predicting the temperature distribution, residual stress and distortion in SYSWELD. The change of current has major effect on the heat input and heat distributed. Thus generated heat has significant effect on the microstructure formation and micro

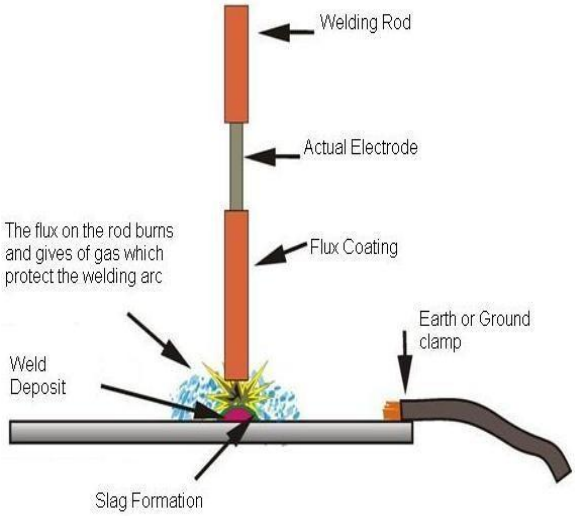


Figure 1 Shielded metal arc welding

hardness and corrosion behavior. Hence it is important to study the effect of heat input by varying the process parameters like current during welding process.

## 2. Experimental Results And Characterization

The heat input were calculated using the expression H.I = VIη/s.

Where, V- Voltage (V), I – current (A), η- efficiency, s- Welding speed (mm/s)

The effect of current on the macro structural formation is presented in the At the lower background current 32 A the heat input was 1207.54 J/mm which was not sufficient to make full penetration. As the background current increased the heat input is increased which cause deeper and shallow weld bead. At heat input 1.91 kJ/mm optimum deep and wide weld bead is achieved. This fact was agreed by the finite element analysis. Further increase of heat input create shallow weld and larger TMAZ region which is not favorable. The excess heat generation of 3622.64 J/mm results porosity in the weld region. In addition the width was so wider than the former case which may decrease the mechanical properties.

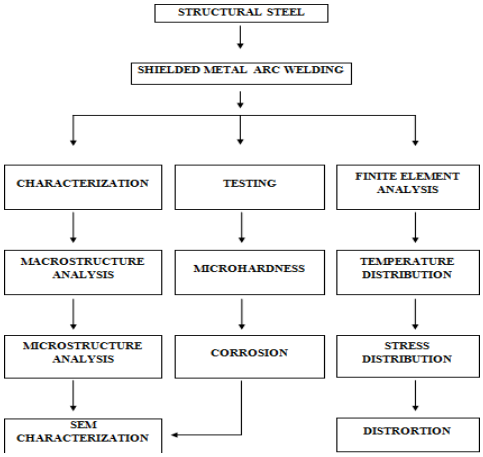


**Table 1**
**Methodology**

The parent material consists of elongated grains having a average grain size in the range -100 µm Weld fusion zones typically exhibit coarse columnar grains because of the prevailing thermal conditions during weld metal.This often results in inferior weld mechanical properties and poor resistance to hot cracking. It is thus highly desirable to control solidification structure in welds and such control is often very difficult because of higher temperatures and higher thermal gradients in welds in relation to castings and the epitaxial nature of the growth process. At 64 A relatively finer microstructure was observed than the other microstructures. This was attributed to the optimum heat generation in the weld region that controls the grain growth. The grain size of HAZ regions are very coarser compare to the weld region. The heats conducted from the weld region provide the activation energy to the grain to grow.

Figure 2 Base material

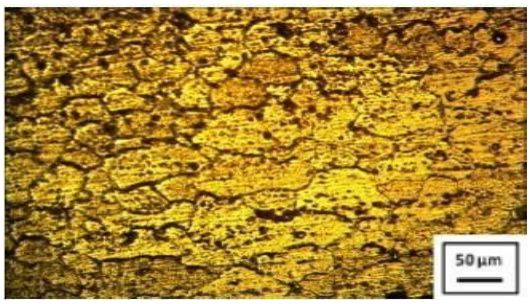

The hardness of the material is dependent on its microstructure. So, hardness measurement would be an acceptable method to investigate the inhomogeneous microstructures. Details of optical microscope's images of the different areas show significant difference in the microstructure of the regions which exhibit high and low hardness values. According to Hall petch relationship, grain size is inversely proportional to the strength or hardness. The base materials have the finer most grains thus it holds higher hardness value. The finer microstructure yields higher hardness due to the increase in the boundary energy. The HAZ region exhibit coarser most grain size thus it obtained lower hardness value. The intermediate grain size (weld region) exhibit intermediate hardness

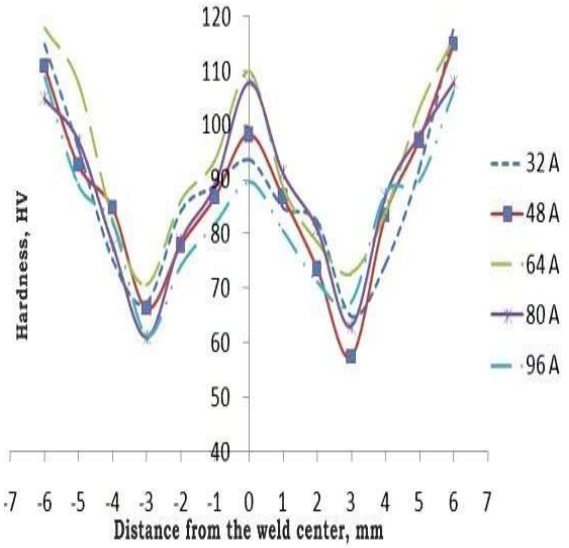


**Figure 3 Microhardness**

Although some alloys can be autogenously welded, filler metals are more commonly used. The use of filler metals with compositions different from the base material may produce an electrochemical potential difference that makes some regions of the weldment more active alloys. For the majority of steel grades, the weld metal and the HAZ become nobler relative to the base metal for a saltwater environment. There are a number of other common weld deposit base metal combinations that are known to form galvanic couples. It is common practice to use austenitic stainless steel welding consumables for field repair of heavy machinery, particularly those fabricated from high-strength low-alloy steel. This practice leaves a cathodic stainless steel weld deposit in electrical contact with the steel. In the presence of corrosive environments, hydrogen is generated at the austenitic weld metal cathode, which is capable of corrosion. In addition the fine microstructure of the weld region results high corrosion.

## 3. Finite Element Methods

**Sysweld capabilities**

From the review of the limited number of commercial finite element codes capable of weld simulations, the SYSWELD finite element code has been found to have the extensive capabilities and dedicated tools for the simulation of welding. These tools include material deposit via element activation/de-activation and pre-defined moving heat sources. Another key feature of the SYSWELD code which sets it apart from other commercial finite element software is the ability to model metallurgical transformations. Metallurgical transformations include volume changes due to phase transformations as well as the change of mechanical properties due to the phase transformations. Also included is a library of metallurgical models for both steel and aluminum. The other more general capabilities include the option to use either 2-D or 3-D models, the ability to perform multiple weld passes, availability of a large range of material behavior laws including elastic- perfectly plastic, isotropic strain hardening, kinematic strain hardening, and finally the use of temperature dependent material properties.

## 4. Finite Element Simulation Of Welding

**Mesh size and time step relationship**

Due to high peak temperatures, large spatial temperature gradients, and rapid temporal temperature fluctuations imposed by the weld heat source, it is necessary to have very small element sizes and consistent time steps. A fine mesh to capture the spatial gradients implies a small time step. That is, it is necessary to choose a time step which is small enough to resolve these large temperature variations for a given mesh. An approximation to the relationship of mesh density to the time step is developed from the heat conduction equation.

Considering the heat conduction equation $\rho C \frac{\delta T}{\delta t} = Q + \frac{\delta}{\delta X}\left(k \frac{\delta T}{\delta X}\right)$ (4.1)

where $k_{ij}$ thermal conductivity W/mK. For an isotropic material with a temperature independent thermal conductivity, no internal heat generation, and heat transfer in one dimension only, say, the x- direction. Then the equation reduces to

$$\rho C \frac{\delta T}{\delta t} = k \frac{\delta^2 T}{\delta \square^2}$$

For the same change in temperature, can be used to estimate the relationship between the spatial and time increments as

$$\Delta t = (\Delta x)^2 \quad (4.3)$$

Where the thermal diffusivity $\kappa = k/(\rho C_p)$. Utilizing the data for Mild Steel at room temperature.Thermal diffusivity K= $11.7*10^{-6}$ $m^2/s$

Assuming a characteristic mesh size of 3 mm, the estimate of the time step is

$$\frac{(3\text{ mm})^2}{11.72 \times 10^{-6} \text{m}^2/\text{S}} \times \left(\frac{\text{mm}}{1000\text{ mm}}\right)^2 = 0.25\ \text{S} \quad (4.4)$$

Therefore, for a characteristic mesh size of 3 mm, a time step of about 0.25 seconds should be sufficient to properly capture the temporal thermal variations in the weld model. Convergence studies utilizing the 3 mm mesh also confirmed a time step of 0.1 seconds yielding numerically acceptable results. These values are relative between two successive iterations. Analyses using a time step of 0.1s proved too time consuming such that the convergence criteria were relaxed to 1.0 on displacement, such that a time step of 0.5 seconds could be used.

**Moving heat sources**

Heat generation in welding is based on the concept of instantaneous heat sources. The heat source model developed by Goldak is used popularly, which distributes the heat throughout the volume of the molten zone. The Goldak heat source model is defined spatially by a double ellipsoid. The front half of the source is the quadrant of one ellipsoidal source, and the rear half is the quadrant of a second ellipsoidal source. The power density distribution is assumed to be Gaussian along the weld path, or the z- axis on the work piece. It is convenient to introduce a coordinate $\xi$ , fixed on the heat source and moving with it.

$$\xi = z + \upsilon(\tau - t)$$

Q is the heat available at the source. For an electric arc the heat available is

Where $\upsilon$ is the welding speed, $\tau$ is a lag time necessary to define the position of heat source at t = 0. In the double ellipsoid model, the fractions of heat deposited in the front and rear of heat source are denoted by $f_f$and $f_r$respectively, and these fractions

$$q(x,y,z,t) = \left(\frac{6\sqrt{3} f_f Q}{abc_1 \pi \sqrt{\pi}}\right) e^{-3(x^2/a^2)} e^{-3(y^2/b^2)} e^{-3(\xi^2/c_1^2)} \quad (4.2)$$

Where $f_f$denotes fraction of heat deposited in front of heat source. a, b, c denotes the semi axes of the ellipsoid parallel to the axes. Q is the heat available at the source.

$$q(x,y,z,t) = \left(\frac{6\sqrt{3} f_r Q}{abc_2 \pi \sqrt{\pi}}\right) e^{-3(x^2/a^2)} e^{-3(y^2/b^2)} e^{-3(\xi^2/c_2^2)} \quad (4.5)$$

Where $f_r$denotes fraction of heat deposited in rear of heat source. a, b, c denotes the semi axes of the ellipsoid parallel to the axes. Q is the heat available at the source.

$$Q = \eta V I \quad (4.6)$$

Where $\eta$ is the heat source efficiency, V, is the arc voltage, and I is the arc current. The parameters *a*, *b*, $c_1$, and $c_2$ are independent, and can take on different values for the front and rear quadrants of the source to properly model the weld arc.

**Specified weld arc model parameters**

As described previously in Section 2.3, the Goldak heat source model is used to simulate the weld arc. The heat source parameters while the values of parameters are tabulated in Table 2

The value of the heat input is calculated by using equation.

V - Voltage in volts
I - Current in Ampere
$\eta$ - Arc efficiency = 80%
Q - Heat input, W

**Governing relations**

The governing differential equation for three dimensional heat conduction equations for a solid in Cartesian coordinate system is given by

$$\frac{\delta}{\delta x}\left(k \frac{\delta T}{\delta x}\right) + \frac{\delta}{\delta y}\left(k \frac{\delta T}{\delta y}\right) + \frac{\delta}{\delta z}\left(k \frac{\delta T}{\delta z}\right) + q_g = \rho C \left(\frac{\delta T}{\delta t}\right) \quad (4.7)$$

are specified to satisfy $f_f + f_r = 2$. Let q denote the power density in W/m$^3$ within the ellipsoid, and let a, b, and c. denote the semi-axes of the ellipsoid parallel to the axes. Then the power density distribution inside the front quadrant is specified .

where $q_g$ is the heat generation per unit volume in W/m$^3$, ρ is density of the material in kg/m$^3$; $C_p$ is specific heat in J/kgK and $k_x$, $k_y$, $k_z$ are thermal conductivity W/mK. respectively along x, y and z directions.Fourier's law of heat conduction relates the heat flux and the temperature gradient by the equation.

$$q = -k \frac{dT}{dx}$$

Where, q is heat flux in W/m$^2$ and k is thermal conductivity in W/mK.

**Table 2 Parameters of Double Ellipsoid Heat Source Model and Calculated Heat Input**

Here ρ, $C_p$ and k depend on temperature and equation (5.6) is non-linear. For isotropic materials, $k = k_x = k_y = k_z$ and the equation (4.7) becomes,

At the solid boundary, velocity of fluid becomes zero and the heat by conduction equals convective heat, which is given by Newton's law of heating / cooling,

$$-k \frac{dT}{dx} = h_c (T_s - T_\infty) \quad (4.13)$$

Where $h_c$ includes the convective and radioactive heat transfer and calculated by Vinokurov's empirical relationship, at all free surfaces

$$h = 2.41 \times 10^{-3} \varepsilon T^{1.61} \quad (4.14)$$

Where ε is emissivity, T is temperature (K), $T_s$ is surface temperature (K), and $T_\infty$ is ambient temperature (K).

## 5 RESULTS AND DISCUSSION

### Finite Element Simulation Of Temperature Distribution Using Sysweld

| Current | Goldak Parameters | | | | Speed, mm/s | Heat input J/mm |
|---|---|---|---|---|---|---|
| | a mm | b mm | $C_1$ mm | $C_2$ mm | | |
| 48 | 2 | 3 | 1.5 | 3 | 1.06 | 1811.15 |
| 64 | 1.5 | 3 | 2 | 3.5 | 1.06 | 2415.09 |
| 80 | 1.75 | 3 | 2.5 | 4 | 1.06 | 3018.86 |

Special Issue on Proceedings of International Conference on Newer Trends and Innovation in Nanotechnology, Materials Science, Science and Technology March 2021. International Journal of Aquatic Science, Vol 12, Issue

$$\frac{\delta^2 T}{\delta^2 T} + \frac{\delta^2 T}{\delta^2 T} + \frac{\delta^2 T}{\delta^2 T} + \frac{q_g}{\alpha} = \rho C \left( \frac{\delta T}{\delta} \right)$$

Where, $\alpha = \frac{k}{\rho C_p}$ = thermal diffusivity of the material. (4.11)

The general solution of equation is obtained by substituting the initial and boundary conditions in the finite element analysis.

The initial condition is defined as

$$T(x, y, z, 0) = T_0 = \text{Constant} \quad (4.12)$$

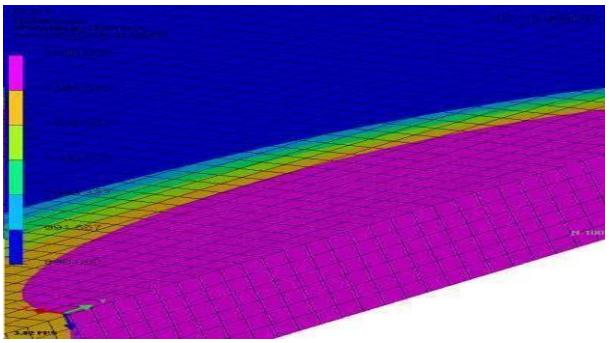

**Figure 4 Weld pool and Temperature Contours for the 1200 W**

Special Issue on Proceedings of International Conference on Newer Trends and Innovation in Nanotechnology, Materials Science, Science and Technology March 2021. International Journal of Aquatic Science, Vol 12, Issue

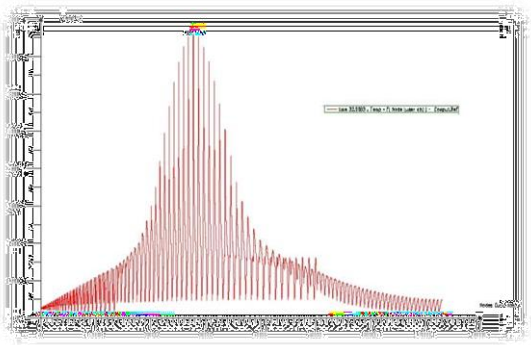

**Figure 5 Nodal Temperature Distributions 1200 W.**

**Finite Element Simulation Of Residual Stresses And Distortion**

After conducting the thermal analysis as mentioned in the previous chapters, the structural analysis is performed. The thermal results are given as inputs to the structural problems, so that the thermo mechanical analysis is performed simultaneously.

A dedicated finite element package for welding SYSWELD was employed for non-linear dynamic structural analysis. Results from thermal analysis form the basis for structural analysis for the prediction of residual stresses and distortion in the plate. The process parameters for calculating the heat input in thermal analysis was retained for structural analysis. Therefore thermal analysis results together with temperature dependent material properties and with proper displacement constraints, structural model was solved and solution is obtained.

A dynamic nonlinear structural Finite Element simulation was performed residual stresses were found at different planes and at different locations..

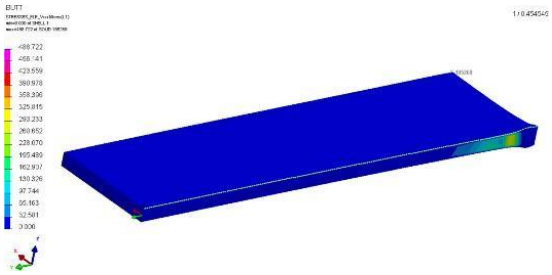

**Figure 6 Contour plot of residual stress distribution at 48 A**

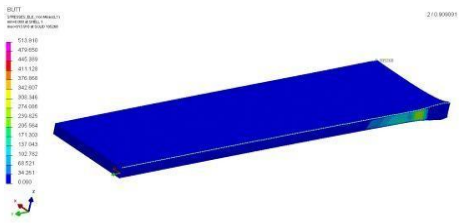

**Figure 7 Contour plot of residual stress distribution at 64 A**

Maximum residual stress for current 64 A is predicted to be 516 N/mm$^{2and}$ distortion is found out to be 0.128mm

Maximum residual Stress for current 80 is predicted to be 593 N/mm$^2$ and distortion is found out to be 0.088mm.

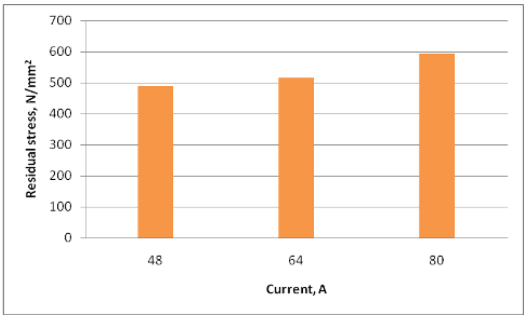


**Figure 8 Variation of Distortion with Change in current**

Increase in the thickness, distortion decreases non linearly. Upon cooling after welding, the weld pool solidifies and shrinks, exerting stresses on the surrounding weld metal and HAZ. The stresses produced from thermal expansion and contraction exceeds the yield strength of the parent metal for various heat source values the effect of heat input with respect to Current on the residual stress and distortion.

## 6. CONCLUSION

A three dimensional finite element model was developed to predict the temperature distribution, residual stresses and distortion.

- Macrostructure examination was carried out to find the width and penetration of the weld bead. Of five heats input condition, current value of 64 A results optimum width to penetration ratio.
- The microstructural investigation shows that the grain sizes in the HAZ are coarser than the weld region.

- Due to increase in boundary energy, the weld region exhibit higher hardness next to base material. A W shaped hardness plot was observed along the cross section.
- The fine grains are more prone for corrosion because of its high sensitivity. Thus the weld region exhibit, higher corrosion than other region.
- A 3-D non-linear transient thermal model was developed to predict the temperature distribution using the concept of Finite Element Method.
- The process was also simulated using SYSWELD.
- Maximum temperature during the experiment was found to be 1650 °C and 1420 °C.
- The developed model was validated with the experimental results and a good agreement was found.
- Structural analysis were made and was able to predict the residual stress and distotion.
- Various Parameters of Goldak equation gives the various bead shape in the base metal.
- Increase in the amount of heat input increses the residual stress and Increase in thickness decrease the thickness value.

## 7. REFERENCES

1. Alok Nayar (2002), 'Steel Handbook', Tata McGraw-Hill publishers, New Delhi.
2. Anca A., Cardona A. and Risso J. (2004), '3D-Thermo-Mechanical Simulation of Welding Processes', International Journal of Mechanical Computational, Vol. 23, pp. 2301-2318.
3. Anderson B.A.B. (1978), 'Thermal stresses in submerged arc welded joint considering phase transformation', Journal of Engineering Materials and Technology, Vol. 100, pp. 356-362.
4. Ansys User Manual: Swanson Analysis Systems, Inc.
5. Barroso A., Canas J., Picon R., Paris F., Mendez C. and Unanue I. (2010), 'Prediction of welding residual stresses and displacements by simplified models and experimental validation', Journal of Materials and Design, Vol. 31, pp. 1338- 1349.
6. Bate S.K.,Charles R.,Warren A.(1999), 'Finite element analysis of a single bead-on- plate specimen using SYSWELD', International Journal of Pressure Vessels and Piping. Vol.86, pp.73-78.
7. Capriccioli Andrea and Frosi Paolo (2009), 'Multipurpose ANSYS FE procedure for welding processes simulation', International Journal of Fusion Engineering and Design, Vol. 84, pp. 546-553.
8. Chang Peng-Hsiang and Teng Tso-Liang (2004), 'Numerical and experimental investigations on the residual stresses of the butt-welded joints', Journal of Computational Materials Science, Vol. 29, pp. 511-522
9. Christensen N. (1965), 'Distribution of temperature in arc welding', British Welding Journal, Vol. 12, pp. 54-57
10. Davis J.R. (1998), 'Metals Handbook', ASM International, 10th Edition, Vol. 6, pp. 789 - 816.
11. Dean Deng, Hidekazu Murakawa and Wei Liang (2007), 'Numerical simulation of welding distortion in large structures', Computer Methods in Applied Mechanics and Engineering, Vol. 196, pp. 4613-4627
12. Deshpande, Tanner D.W.J, Sun W., Hyde T .H., and McCartney G. (2005), 'Combined butt joint welding and post weld heat treatment simulation using SYSWELD and ABAQUS"Journal of Design and Applications,Vol. 225, pp. 84-93
13. Gatto A., Bassoli E. and Fornari M. (2004), 'Plasma Transferred Arc deposition of powdered high performances alloys: process parameters optimisation as a function of alloy and geometrical configuration', Surface and Coatings Technology, Vol. 187, pp. 265– 271.
14. Goldak J. and Akhlaghi M. (2005), 'A text book of Computational Welding Mechanics', Springer Publications.
15. Goldak J., Chakravarti A. and Bibby M. (1984), 'A New Finite Element Model for Welding Heat Sources', Metallurgical Transactions B, Vol. 15B, pp. 229 - 305.
16. Gunaraj V. and Murugan N. (2000), 'Prediction and Optimization of Weld Bead Volume for the Submerged Arc Process'- Part 2, Welding Research Supplement, Vol. 79, pp.331s-338s.
17. Guo W. and Kar A. (2000), 'Determination of weld pool shape and temperature distribution by solving three-dimensional phase change heat conduction problem', Science and Technology of Welding and Joining, Vol. 5, pp. 317-323.